ACS Energy LETTERS

http://pubs.acs.org/journal/aelccp

Blade-Coatable Hexagonal Boron Nitride Ionogel Electrolytes for Scalable Production of Lithium Metal Batteries

Cory M. Thomas, Woo Jin Hyun, Hsien Cheng Huang, Davy Zeng, and Mark C. Hersam*

Cite This: *ACS Energy Lett.* 2022, 7, 1558–1565

Read Online

ACCESS | Metrics & More | Article Recommendations | Supporting Information

ABSTRACT: Solid-state electrolytes have attracted significant attention for rechargeable lithium-ion batteries due to their potential to enable higher energy density technologies and improve cell safety by removing volatile liquid electrolytes. However, existing solid-state electrolyte materials lack sufficient electrochemical performance or require expensive and time-consuming processing methods that have prevented their wide-scale adoption. Here, a blade-coatable hexagonal boron nitride ionogel electrolyte is introduced that exhibits high room temperature ionic conductivity (>1 mS cm^{-1}), is stable against lithium metal anodes, and can be applied over a wide area in a thin (<40 μm) and crack-free film. Furthermore, this blade-coatable slurry has a tunable viscosity to enable its use in existing battery manufacturing infrastructure. The resulting blade-coated hBN ionogel electrolyte is employed in a lithium metal battery with a $LiFePO_4$ cathode, exhibiting superlative rate capability at room temperature with a 78% capacity retention after 500 cycles at a rate of 1C.

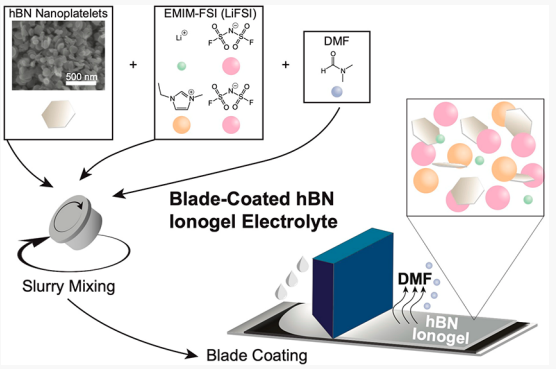

Next-generation energy storage technologies are necessary to fulfill the ever-increasing demands for electric vehicles, grid-level energy storage, and portable electronic devices.[1] Although traditional lithium-ion batteries are widely available, they suffer from limitations in energy density and poor safety due to the use of a volatile liquid electrolyte.[2,3] In recent years, lithium metal anodes have gained interest since they offer an exceptionally high theoretical specific capacity (3860 mAh g^{-1}) that is an order of magnitude higher than incumbent graphitic anode materials (372 mAh g^{-1}).[4−6] However, traditional organic liquid electrolytes, when combined with a lithium−metal anode, are susceptible to poor cycling stability and dendritic lithium growth, which can result in internal short circuits and catastrophic failure.[7] As a result, significant attention has been devoted to solid-state electrolytes (SSEs) that enable the use of lithium metal anodes while concurrently minimizing flammability concerns by using nonvolatile components.[8−12] Despite this promise, state-of-the-art SSEs suffer from a combination of pitfalls including poor room-temperature ionic conductivity, unstable interfaces with lithium-ion battery electrode materials, and expensive, nonscalable processing methods that have limited commercial viability.[13]

Recent efforts have attempted to address the processing limitations of SSEs to enable their introduction into mass-produced lithium metal battery (LMB) applications.[14,15] Specifically, it is necessary that the production of SSEs yields a thin layer (<50 μm) to maintain sufficiently high cell-level energy densities.[16] Since blade coating is a widely used and well-understood additive manufacturing method that is currently used to produce lithium-ion batteries, it is of high interest to develop blade-coatable SSE slurries.[17] Several reports have used blade coating to demonstrate its potential for SSE materials including polymer composites,[18,19] sulfides,[20−22] ceramics,[23] and sol−gel ionogels.[24] However, these reported examples possess one or more significant drawbacks such as poor room-temperature ionic conductivity, energy and time intensive post-processing, or instability with lithium metal anodes, cathode electrode materials, or ambient air. In contrast, nanocomposite ionogels, consisting of an ionic liquid and an inorganic nanomaterial, offer several advantages that can potentially resolve these issues.[25,26] For example, prior work has shown that hexagonal boron nitride (hBN)

Received: March 5, 2022
Accepted: March 28, 2022
Published: March 30, 2022

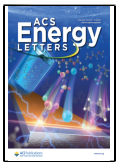

Downloaded via UNIV OF CHICAGO on December 10, 2022 at 03:23:18 (UTC).
See https://pubs.acs.org/sharingguidelines for options on how to legitimately share published articles.

ACS Publications © 2022 American Chemical Society

https://doi.org/10.1021/acsenergylett.2c00535
ACS Energy Lett. 2022, 7, 1558−1565

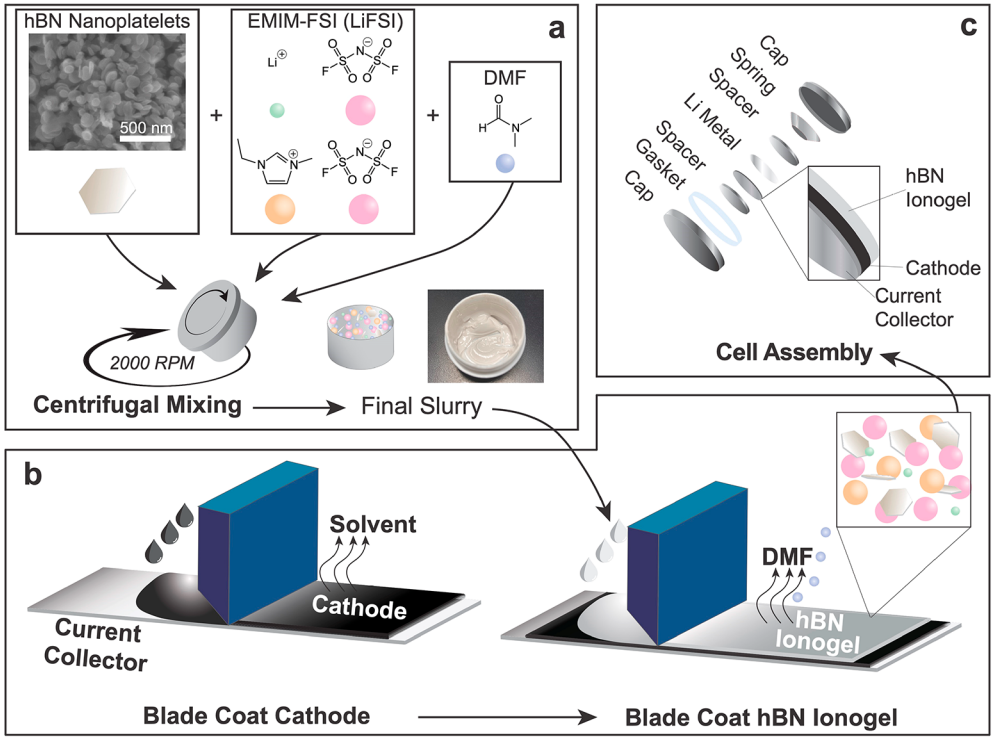

Figure 1. Schematic illustration of the all-solid-state battery construction using the blade-coated hBN ionogel electrolyte. (a) hBN nanoplatelets mixed with ionic liquid electrolyte (EMIM-FSI (3.5 M LiFSI)) and a diluent solvent (DMF). (b) Cathode composite blade-coated, dried, and pressed before the hBN ionogel slurry is blade-coated and dried, leaving a thin SSE film on the cathode. (c) Electrolyte-coated cathode is then assembled with a lithium metal anode and sealed inside the cell casing.

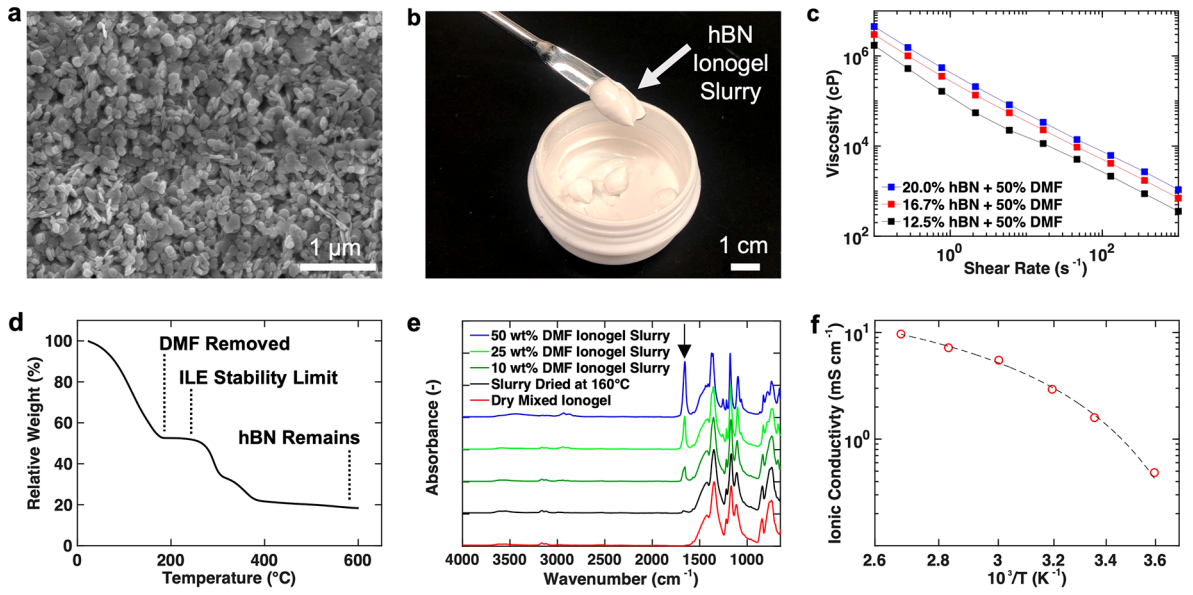

Figure 2. Blade-coatable hBN ionogel slurry. (a) Scanning electron microscopy (SEM) of the exfoliated hBN nanoplatelets. (b) Photograph of the final blade-coatable hBN ionogel slurry including 16.7 wt % hBN, 33.3 wt % EMIM-FSI (3.5 M LiFSI), and 50 wt % DMF as prepared by centrifugal mixing with zirconia mixing balls. (c) Ionogel slurry viscosity as a function of shear rate and varying hBN content. (d) TGA of the blade-coatable hBN ionogel slurry showing full removal of the DMF solvent at ∼170 °C and the degradation of the ILE at ∼225 °C, leaving only the hBN nanoplatelets at higher temperatures. (e) FTIR spectra of various hBN ionogel slurry samples in addition to a dry mixed hBN ionogel control. The initial slurry content of DMF (50 wt %) is reduced by >99% after drying at 160 °C for 30 min as evidenced by the reduction in the peak height of the DMF carbonyl stretch at 1670 cm^{-1}.[37] (f) Temperature dependence of ionic conductivity in the hBN ionogel (33.4 wt % hBN and 66.6 wt % EMIM-FSI (3.5 M LiFSI)). The dashed line is a Vogel−Fulcher−Tammann (VFT) model fit to $\sigma = A \exp[-B(T - T_0)]$, where A, B, and T_0 are 48.8 mS cm^{-1}, 231 K^{-1}, and 229 K, respectively.

nanoplatelets produced using a scalable liquid-phase exfoliation process are suitable ionogel matrix materials, resulting in excellent thermal stability, high ionic conductivity (>1 mS cm^{-1}), favorable mechanical modulus (>1 MPa), and a wide

https://doi.org/10.1021/acsenergylett.2c00535
ACS Energy Lett. 2022, 7, 1558−1565

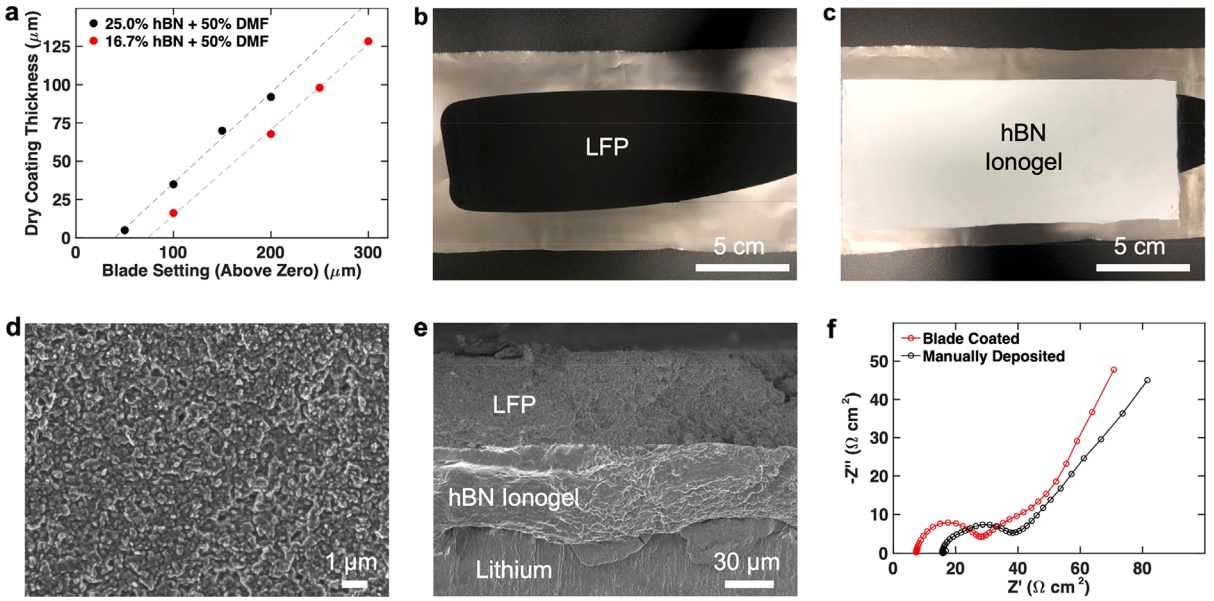

Figure 3. Blade-coated hBN ionogel. (a) Blade-coated hBN ionogel thickness measured by laser profilometry plotted as a function of the blade height setting. LFP electrodes were blade coated with the hBN ionogel slurry and then dried at 160 °C for 30 min before the height measurement. (b) Photograph of an LFP electrode blade-coated onto an aluminum current collector. (c) Blade-coated hBN ionogel on the same LFP cathode. (d) SEM image of the blade-coated hBN ionogel slurry on an LFP cathode. (e) Cross-sectional SEM micrograph of an LFP|Li cell showing the hBN ionogel thickness and close interfacial contact to the LFP and Li electrodes. (f) Electrochemical impedance spectroscopy (EIS) of LFP|Li cells comparing the impedance of the hBN ionogel electrolyte applied by blade coating or by manual deposition with a spatula and razor blade.

electrochemical stability window.[27,28] Despite these advantages, a blade-coatable inorganic ionogel electrolyte without time-consuming in situ gel formation has not yet been reported.

Herein, we disclose the formulation of an hBN ionogel slurry that yields a thin (<40 μm) blade-coated SSE. A carefully selected diluent solvent (i.e., *N*,*N*-dimethylformamide (DMF)) is used to reduce the viscosity of the ionogel to match that of existing commercial blade-coating slurries used in high-throughput coating equipment. The resulting slurry can be coated directly onto cathode composite electrodes, providing excellent interfacial contact with low impedance. Subsequently, after the diluent solvent is thermally removed, the thin hBN ionogel layer is free of cracks without the use of a polymeric binder, thus maintaining high ionic conductivity and mechanical modulus. These superlative properties are used to demonstrate best-in-class LMB rate capability and cycle stability using a $LiFePO_4$ (LFP) cathode at room temperature.

Figure 1 displays a schematic of the hBN ionogel slurry preparation, application, drying, and use in an LMB. The slurry consisting of hBN nanoplatelets (16.7 wt %), an ionic liquid electrolyte (ILE, 33.3 wt %), and diluent solvent (50 wt %) was prepared via centrifugal mixing to fully homogenize the slurry. The ILE used in the slurry was 1-ethyl-3-methyl-imidazolium bis(fluorosulfonyl)imide (EMIM-FSI) containing 3.5 M (50 mol %) lithium bis(fluorosulfonyl)imide (LiFSI) salt. EMIM-FSI was chosen due to the relatively low viscosity and high ionic conductivity of the imidazolium cation,[29,30] while the FSI anion has been shown to provide cathodic stability down to 0 V vs Li/Li^+.[31,32] Furthermore, a high concentration of LiFSI within an ILE enhances the stability of lithium plating[33] and generates a favorable LiF-rich solid electrolyte interface (SEI) with lithium metal.[34] Nanoplatelets of hBN (Figure 2a), prepared by scalable liquid-phase exfoliation, were used as the gelling matrix due to their desirable physical properties including thermal stability, chemical inertness, electrically insulating nature, and mechanical robustness.[35] Moreover, the insulating nature of the hBN nanoplatelets prevents any undesired electrochemical reactions between the matrix and lithium ions in the electrolyte along with inhibiting any deleterious leakage current across the cell. In addition, the high surface area of the hBN nanoplatelets has been shown to generate strong interactions with the ILE, thus confining the ionic liquid and generating a high mechanical modulus gel (>1 MPa).[27]

The diluent solvent used in the slurry must be sufficiently polar to create a well-mixed slurry (Supporting Information Figure S1) as well as provide favorable thermodynamic properties for thermal removal. DMF possesses sufficient polarity to mix and disperse the hBN ionogel (Figure 2b and Figure S1a), whereas nonpolar solvents such as heptane and toluene (Figures S1b,c) are ineffective. Moreover, nonpolar solvents are immiscible with the ILE, creating phase separation between the ionogel and diluent solvent. The attributes of DMF allow for a range of slurry viscosities that are tuned on the basis of the relative content of the hBN gelling matrix (Figure 2c) and diluent solvent (Figure S2). If the hBN loading is fixed at 16.7 wt %, Figure S3 shows that the viscosity of the hBN ionogel slurry can be tuned with the diluent solvent (50 wt % DMF) to match that of commercial cathode composite slurries,[36] especially at the high shear rates that are relevant to the rapid coating conditions used in existing lithium-ion battery manufacturing infrastructure. Furthermore, an additional advantage of DMF is its boiling point (T_b = 153 °C), which is sufficiently high to prevent undesired excess evaporation at room temperature (unlike 1,4-dioxane (T_b = 101 °C) shown in Figure S1d), but still well below the thermal degradation limit of the ILE. Figure 2d presents the

https://doi.org/10.1021/acsenergylett.2c00535
ACS Energy Lett. 2022, 7, 1558−1565

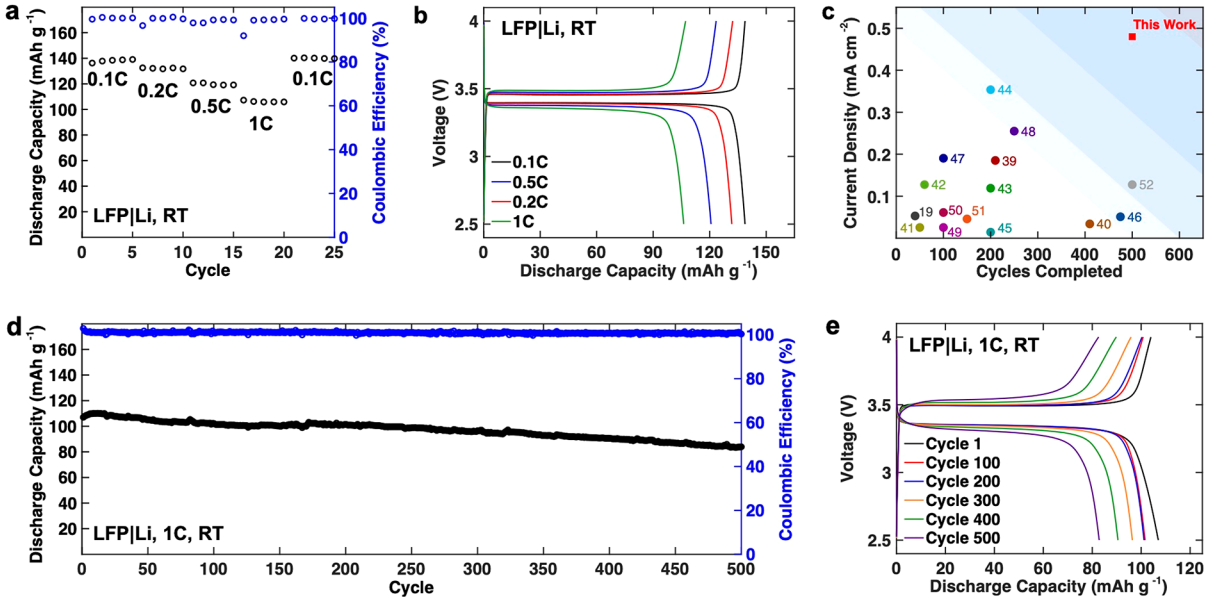

Figure 4. Electrochemical performance of the blade-coated hBN ionogel (33.4 wt % hBN and 66.6 wt % EMIM-FSI (3.5 M LiFSI)) in LFP|Li cells at room temperature (22 °C). (a) Rate capability at various charge/discharge rates and (b) corresponding voltage profiles of the cells. (c) Comparison of recently published reports based on cycling stability of LFP|Li cells with thin (<100 μm) SSEs operating at 20−30 °C. Cycles completed refers to the maximum number of cycles reported during cycle stability testing at a given current density. The number labels indicate the citation number. (d) Room-temperature cycling performance of LFP|Li cells with the blade-coated hBN ionogel electrolyte at a charge/discharge rate of 1C. (e) Selected charge/discharge voltage profiles from the 1C rate LFP|Li cycling test.

thermogravimetric analysis (TGA) of the hBN ionogel slurry, which shows that DMF is fully removed at ∼170 °C, prior to the onset of thermal degradation of EMIM-FSI and LiFSI at ∼225 °C, above which only the hBN nanoplatelets remain intact. Other polar solvents such as *N*-methylpyrrolidone (NMP; T_b = 202 °C) or ethyl lactate (EL; T_b = 154 °C) also mix well with the hBN ionogel (Figures S1e,f). However, the boiling point of NMP is excessively high for efficient thermal removal, while EL is a protic solvent that reacts rapidly with lithium metal anodes. Fourier transform infrared (FTIR) spectroscopy can be used to measure the residual DMF in the resulting hBN ionogel after thermal drying (Figure 2e). Heating the coated slurry at 160 °C for 30 min is sufficient to remove >99% of the diluent solvent as calculated using the peak height for the DMF carbonyl stretch at 1670 cm^{-1}.[37] This rapid removal of the diluent solvent occurs without the introduction of additional FTIR peaks, suggesting the absence of degradation products. The final blade-coated hBN ionogel (33.4 wt % hBN) maintains both a high room temperature ionic conductivity of 1.6 mS cm^{-1} (Figure 2f and Figure S4) and desirable mechanical properties such as a high mechanical modulus exceeding 1 MPa (Figure S5). The storage modulus of the gel is consistently higher than the loss modulus across the entire range of frequency, indicating the solid nature of the hBN ionogel electrolyte.

To ensure that a blade-coated SSE is viable for LMB applications, the material must produce a high-quality film with controllable thickness. To investigate the blade-coating performance of the formulated hBN ionogel slurry, the final thickness of the hBN ionogel films was measured using laser profilometry for various blade settings. The resulting calibration curve (Figure 3a) shows a linear response between the blade setting and final coating thickness over the range of 5−125 μm. Panels b and c of Figure 3 display images of a blade-coated LFP cathode composite on an aluminum current collector before and after blade coating of the hBN ionogel. The dried hBN ionogel is crack-free over large areas as confirmed by optical microscopy (Figure S6). This cohesive film was achieved without the use of a polymeric binder, which is a key advantage since the use of a polymeric binder would compromise the thermal stability of the SSE in addition to diluting the percolating network of the high ionic conductivity ILE and thus decreasing ionic conductivity. The crack-free ionogel film can be attributed to the confinement of the ILE by the hBN nanoplatelets as shown by SEM (Figure 3d). This confinement results in the viscoelastic nature of the film, allowing it to accommodate the removal of the diluent solvent.

The final thickness and interfacial impedance of the blade-coated hBN ionogel were investigated since these parameters determine the energy density and rate performance of LMB cells. Since a preliminary study of bladed-coated hBN ionogel film thickness revealed no significant advantage in rate performance or cell impedance for thicknesses below 100 μm, a final thickness was chosen below the desired maximum of 50 μm for cells with high specific capacity but sufficiently thick to provide protection against incidental short circuiting. A cross-sectional SEM micrograph of a blade-coated LFP|ionogel|Li cell stack is provided in Figure 3e. This image shows that the final thickness of the blade-coated hBN ionogel is ∼40 μm, which is within the desired regime for thin SSE films in high energy density LMB cells (<50 μm). Furthermore, excellent interfacial contact is observed between the hBN ionogel and the LFP cathode composite film. Similarly, the hBN ionogel film achieves high conformality with the lithium metal anode and its surface variations. Electrochemical impedance spectroscopy (EIS) was then used to quantify the interfacial impedance of an LFP|Li cell containing a blade-coated hBN ionogel film compared to an hBN ionogel layer manually deposited using a spatula and razor blade (Figure 3f). Equivalent circuit modeling of the EIS results (Figure S7)

https://doi.org/10.1021/acsenergylett.2c00535
ACS Energy Lett. 2022, 7, 1558−1565

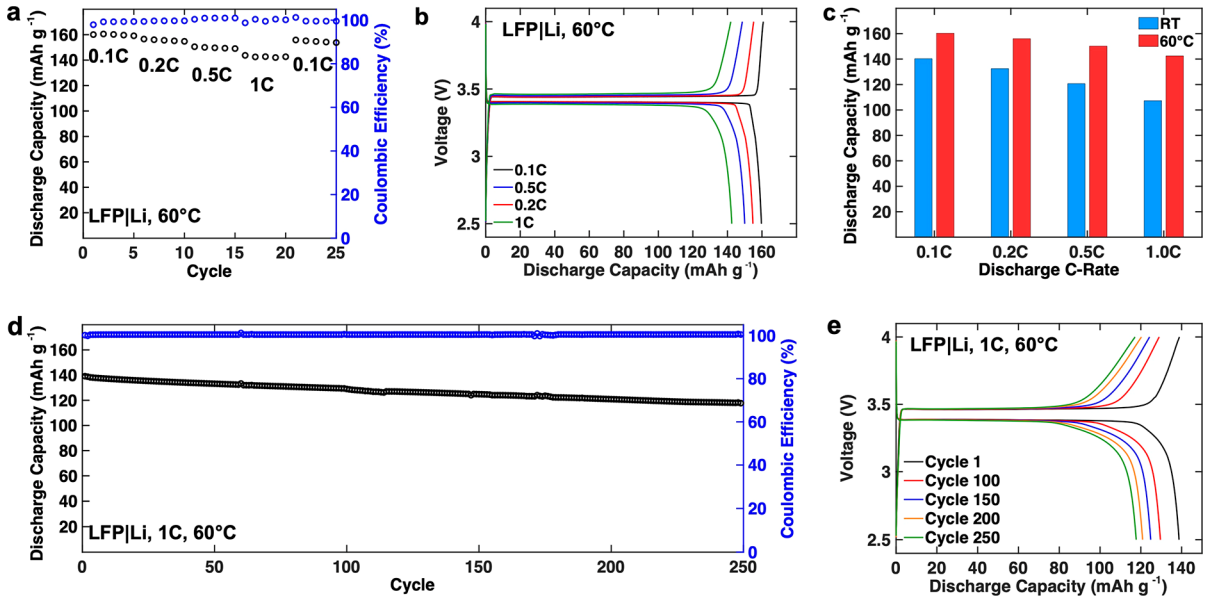

Figure 5. High-temperature (60 °C) performance of LFP|Li cells with the blade-coated hBN ionogel (33.4 wt % hBN and 66.6 wt % EMIM-FSI (3.5 M LiFSI)). (a) Rate capability at various charge/discharge rates and (b) associated voltage profiles at 60 °C operation. (c) Comparison of discharge capacity for room temperature and 60 °C operation at various C-rates. (d) High-temperature cycling stability of an LFP|Li cell with the blade-coated hBN ionogel electrolyte at a charge/discharge rate of 1C. (e) Selected charge/discharge voltage profiles from the cycling stability testing of LFP|Li cells.

reveals that the bulk resistance of the blade-coated ionogel is approximately half of the manually deposited version (9 Ω cm^2 vs 19 Ω cm^2), which is consistent with the blade-coated film being significantly thinner (40 μm vs 300 μm). The superior interfacial contact of the blade-coated hBN ionogel also yields a 20% lower interfacial impedance compared to the manually deposited hBN ionogel, resulting in a lower overall cell impedance.

To confirm the electrochemical stability of the hBN ionogel against lithium metal, cyclic voltammetry (CV) was performed on stainless-steel (SS)|ionogel|Li cells between −0.2 and 3.0 V vs Li/Li^+. The resulting voltammogram (Figure S8) displays only one reversible anodic and cathodic peak pair that corresponds to lithium plating and stripping. Furthermore, negligible change in current density is observed over five cycles, indicating stability of the ILE with lithium metal, which is consistent with previous reports.[28,31] Moreover, an additional advantage to the high-concentration ILE within the hBN ionogel is enhanced anodic stability. Figure S9 shows the results of linear sweep voltammetry (LSV) from 3 to 6 V vs Li/Li^+ using a SS|hBN ionogel|Li cell. The LSV curves compare hBN ionogels containing 3.5 and 1 M LiFSI with the high-concentration ILE exhibiting higher anodic stability (~4.5 V vs Li/Li^+) compared to the reference sample, which matches previous reports of high-concentration electrolytes.[38] Given the anodic stability limit of the hBN ionogel, it is well-suited to be paired with an LFP cathode within an LMB. Therefore, cyclic voltammetry was performed on an LFP|ionogel|Li cell between the voltage cutoffs of 2.5 and 4.0 V. The resulting voltammogram (Figure S10) displays a set of anodic and cathodic peaks representing lithiation and delithiation of the LFP with consistent peak current density after five cycles. This result further confirms the electrochemical stability of the blade-coated ionogel within an LFP|Li cell structure.

To test the cycling stability and rate performance of the blade-coated hBN ionogel, LFP|Li cells were constructed and galvanostatically cycled at room temperature (Figure 4). Figure 4a displays the rate test of the LFP|Li cells with the blade-coated hBN ionogel, which yields the expected gravimetric capacity of 140 mAh g^{-1} at 0.1C and an excellent high-rate performance of 106 mAh g^{-1} at 1C. The charge and discharge profiles at various C-rates are shown in Figure 4b, and the expected LFP voltage plateaus at ~3.45 and ~3.39 V indicate stable electrochemical operation in the cell. To test the cycling stability of the blade-coated hBN ionogel, LFP|Li cells were cycled continuously at 1C (Figure 4d,e). After 500 cycles, the capacity retention was 78% with an average Coulombic efficiency of >99.99%. Significantly, the long-term cycling stability test yielded no voltage fluctuations or short circuits due to lithium dendrites, thus confirming the dendrite resistance of the hBN ionogel. Furthermore, Figure 4c compares this result with the cycling stability of recently published work[19,39−52] using an LFP|Li structure, thin (<100 μm) SSE, and room-temperature cycling. Evidently, the combination of high ionic conductivity and robust mechanical properties of the blade-coated hBN ionogel results in best-in-class cycling stability at the highest areal current density. Although the data presented here use an LFP cathode, the blade-coated hBN ionogel approach can be expanded to higher voltage cathode materials using a layered heterostructure of multiple ionogels as described in a previous report.[28]

To demonstrate the thermal stability of the blade-coated hBN ionogel, the rate performance and cycling stability of LFP|Li cells were tested at an operating temperature of 60 °C (Figure 5). Due to the increased ionic conductivity at elevated temperatures (Figure 2f) and further infiltration of the ILE into the LFP cathode, the achievable gravimetric capacity increased significantly to 160.5 mAh g^{-1} at 0.1C and 142.7 mAh g^{-1} at 1C, while maintaining an average Coulombic efficiency > 99.8%. These results represent increases in gravimetric capacity of 14 and 33% at 0.1C and 1C, respectively. Furthermore, the charge and discharge plateaus are well-behaved but exhibit

https://doi.org/10.1021/acsenergylett.2c00535
ACS Energy Lett. 2022, 7, 1558−1565

reduced polarization, indicating a lower overpotential (Figure 5b) during high-temperature operation. The high-temperature cycling stability of the blade-coated hBN ionogel was tested through galvanostatic cycling of LFP|Li cells at 60 °C with a 1C charge and discharge rate (Figures 5d,e). The resulting capacity retention was 85% after 250 cycles with an average Coulombic efficiency > 99.9%. These attributes display the ability of the blade-coated hBN ionogel electrolyte to perform beyond the temperature limitations of traditional organic liquid electrolytes.

In conclusion, we have developed a blade-coatable hBN ionogel slurry that yields thin, conformal solid-state electrolyte films for high-performance LMBs. Compared to other potential SSE technologies, this platform allows for the use of existing lithium-ion battery manufacturing infrastructure without requiring expensive and time-intensive processing steps. Using a DMF diluent solvent, the viscosity of the hBN ionogel slurry can be tuned to match that of commercially coated materials and only requires a brief thermal treatment to remove the solvent. The blade-coated hBN ionogel can be applied in a thin (<40 μm) and crack-free film, enabling the production of high energy density LMB cells. Additionally, the resulting hBN ionogel electrolyte has sufficient mechanical stiffness to inhibit the growth of lithium dendrites with a storage modulus > 1 MPa, while also providing excellent interfacial contact to composite cathodes and lithium metal anodes. Beyond these favorable mechanical properties, the ionic conductivity of the hBN ionogel remains high with values of 1.6 and 5.5 mS cm^{-1} at room temperature and 60 °C, respectively. The resulting high-performance SSE is also electrochemically stable against lithium metal, enabling its utilization in LFP|Li cells that can be cycled at 1C rate with a 78% capacity retention after 500 cycles at room temperature. Additionally, the thermal stability of the hBN nanoplatelets and ILE allows for operation of LFP|Li cells at 60 °C with a 33% improvement in gravimetric capacity at 1C compared to room temperature. Although these performance tests were performed in a coin cell format, the large-area uniformity of blade-coated hBN ionogels will allow them to be applied to alternative battery geometries (e.g., pouch cells) as they progress toward industrial-scale demonstrations. Overall, this work establishes blade-coated hBN ionogels as an attractive and scalable option for LMB solid-state electrolytes.

■ ASSOCIATED CONTENT

Supporting Information

The Supporting Information is available free of charge at https://pubs.acs.org/doi/10.1021/acsenergylett.2c00535.

Experimental methods, photographs of ionogel slurries, ionogel slurry viscosity, EIS spectra, ionogel rheology, equivalent circuit modeling results, cyclic voltammetry, linear sweep voltammetry, and precycling data (PDF)

■ AUTHOR INFORMATION

Corresponding Author

Mark C. Hersam − *Department of Materials Science and Engineering, Department of Chemistry, and Department of Electrical and Computer Engineering, Northwestern University, Evanston, Illinois 60208, United States;* orcid.org/0000-0003-4120-1426; Email: m-hersam@northwestern.edu; https://www.hersam-group.northwestern.edu/

Authors

Cory M. Thomas − *Department of Materials Science and Engineering, Northwestern University, Evanston, Illinois 60208, United States*

Woo Jin Hyun − *Department of Materials Science and Engineering, Northwestern University, Evanston, Illinois 60208, United States;* Present Address: Department of Materials Science and Engineering, Guangdong Technion - Israel Institute of Technology, Shantou, Guangdong 515063, China

Hsien Cheng Huang − *Department of Materials Science and Engineering, Northwestern University, Evanston, Illinois 60208, United States*

Davy Zeng − *Department of Materials Science and Engineering, Northwestern University, Evanston, Illinois 60208, United States*

Complete contact information is available at: https://pubs.acs.org/10.1021/acsenergylett.2c00535

Notes

The authors declare no competing financial interest.

■ ACKNOWLEDGMENTS

This work was primarily supported by the NSF Future Manufacturing Program (CMMI-2037026). In addition, C.M.T. is supported by the National Science Foundation Graduate Research Fellowship under Grant No. DGE-1842165. The preparation of the hBN nanoplatelets was supported by the U.S. Department of Commerce, National Institute of Standards and Technology (Award 70NANB19H005) as part of the Center for Hierarchical Materials Design (CHiMaD). Scanning electron microscopy and FTIR analyses were performed in the NUANCE facility at Northwestern University, which is supported by the Soft and Hybrid Nanotechnology Experimental (SHyNE) Resource (NSF ECCS-1542205), the Materials Research Science and Engineering Center (NSF DMR-1720139), the State of Illinois, and Northwestern University. Rheometry and laser profilometry were performed in the MatCI facility, which receives support from the Materials Research Science and Engineering Center (NSF DMR-1720139).

■ REFERENCES

(1) Mann, M.; Babinec, S.; Hendrickson, S.; Ho, H.; Spitsen, P. *Energy Storage Grand Challenge: Energy Storage Market Report*; DOE/GO-102020−5497; U.S. Department of Energy, Washington, DC, USA, 2020; https://www.energy.gov/energy-storage-grand-challenge/downloads/energy-storage-market-report-2020 (accessed 2021-08-10).

(2) Van Noorden, R. The Rechargeable Revolution: A Better Battery. *Nature* **2014**, *507* (7490), 26−28.

(3) Liu, K.; Liu, Y.; Lin, D.; Pei, A.; Cui, Y. Materials for Lithium-ion Battery Safety. *Sci. Adv.* **2018**, *4* (6), eaas9820.

(4) Lin, D.; Liu, Y.; Cui, Y. Reviving the Lithium Metal Anode for High-Energy Batteries. *Nat. Nanotechnol.* **2017**, *12* (3), 194−206.

(5) Liu, B.; Zhang, J.-G.; Xu, W. Advancing Lithium Metal Batteries. *Joule* **2018**, *2* (5), 833−845.

(6) Cheng, X.-B.; Zhang, R.; Zhao, C.-Z.; Zhang, Q. Toward Safe Lithium Metal Anode in Rechargeable Batteries: A Review. *Chem. Rev.* **2017**, *117* (15), 10403−10473.

(7) Tarascon, J. M.; Armand, M. Issues and Challenges Facing Rechargeable Lithium Batteries. *Nature* **2001**, *414* (6861), 359−367.

(8) Zheng, F.; Kotobuki, M.; Song, S.; Lai, M. O.; Lu, L. Review on Solid Electrolytes for All-Solid-State Lithium-Ion Batteries. *J. Power Sources* **2018**, *389*, 198−213.
(9) Wang, C.; Fu, K.; Kammampata, S. P.; McOwen, D. W.; Samson, A. J.; Zhang, L.; Hitz, G. T.; Nolan, A. M.; Wachsman, E. D.; Mo, Y.; et al. Garnet-Type Solid-State Electrolytes: Materials, Interfaces, and Batteries. *Chem. Rev.* **2020**, *120* (10), 4257−4300.
(10) Lau, J.; DeBlock, R. H.; Butts, D. M.; Ashby, D. S.; Choi, C. S.; Dunn, B. S. Sulfide Solid Electrolytes for Lithium Battery Applications. *Adv. Energy Mater.* **2018**, *8* (27), 1800933.
(11) Ngai, K. S.; Ramesh, S.; Ramesh, K.; Juan, J. C. A Review of Polymer Electrolytes: Fundamental, Approaches and Applications. *Ionics* **2016**, *22* (8), 1259−1279.
(12) Manthiram, A.; Yu, X.; Wang, S. Lithium Battery Chemistries Enabled by Solid-State Electrolytes. *Nat. Rev. Mater.* **2017**, *2* (4), 16103.
(13) Duffner, F.; Kronemeyer, N.; Tübke, J.; Leker, J.; Winter, M.; Schmuch, R. Post-Lithium-Ion Battery Cell Production and Its Compatibility with Lithium-Ion Cell Production Infrastructure. *Nat. Energy* **2021**, *6* (2), 123−134.
(14) Huang, K. J.; Ceder, G.; Olivetti, E. A. Manufacturing Scalability Implications of Materials Choice in Inorganic Solid-State Batteries. *Joule* **2021**, *5* (3), 564−580.
(15) Tan, D. H. S.; Banerjee, A.; Chen, Z.; Meng, Y. S. From Nanoscale Interface Characterization to Sustainable Energy Storage Using All-Solid-State Batteries. *Nat. Nanotechnol.* **2020**, *15* (3), 170−180.
(16) Wu, J.; Yuan, L.; Zhang, W.; Li, Z.; Xie, X.; Huang, Y. Reducing the Thickness of Solid-State Electrolyte Membranes for High-Energy Lithium Batteries. *Energy Environ. Sci.* **2021**, *14* (1), 12−36.
(17) Ding, X.; Liu, J.; Harris, T. A. L. A Review of the Operating Limits in Slot Die Coating Processes. *AIChE J.* **2016**, *62* (7), 2508−2524.
(18) Sheng, O.; Jin, C.; Luo, J.; Yuan, H.; Fang, C.; Huang, H.; Gan, Y.; Zhang, J.; Xia, Y.; Liang, C.; et al. Ionic Conductivity Promotion of Polymer Electrolyte with Ionic Liquid Grafted Oxides for All-Solid-State Lithium−Sulfur Batteries. *J. Mater. Chem. A* **2017**, *5* (25), 12934−12942.
(19) Yu, R.; Bao, J.-J.; Chen, T.-T.; Zou, B.-K.; Wen, Z.-Y.; Guo, X.-X.; Chen, C.-H. Solid Polymer Electrolyte Based on Thermoplastic Polyurethane and Its Application in All-Solid-State Lithium Ion Batteries. *Solid State Ion.* **2017**, *309*, 15−21.
(20) Riphaus, N.; Strobl, P.; Stiaszny, B.; Zinkevich, T.; Yavuz, M.; Schnell, J.; Indris, S.; Gasteiger, H. A.; Sedlmaier, S. J. Slurry-Based Processing of Solid Electrolytes: A Comparative Binder Study. *J. Electrochem. Soc.* **2018**, *165* (16), A3993−A3999.
(21) Ates, T.; Keller, M.; Kulisch, J.; Adermann, T.; Passerini, S. Development of an All-Solid-State Lithium Battery by Slurry-Coating Procedures Using a Sulfidic Electrolyte. *Energy Storage Mater.* **2019**, *17*, 204−210.
(22) Lee, K.; Kim, S.; Park, J.; Park, S. H.; Coskun, A.; Jung, D. S.; Cho, W.; Choi, J. W. Selection of Binder and Solvent for Solution-Processed All-Solid-State Battery. *J. Electrochem. Soc.* **2017**, *164* (9), A2075−A2081.
(23) Jiang, Z.; Wang, S.; Chen, X.; Yang, W.; Yao, X.; Hu, X.; Han, Q.; Wang, H. Tape-Casting $Li_{0.34}La_{0.56}TiO_3$ Ceramic Electrolyte Films Permit High Energy Density of Lithium-Metal Batteries. *Adv. Mater.* **2020**, *32* (6), 1906221.
(24) Guyomard-Lack, A.; Abusleme, J.; Soudan, P.; Lestriez, B.; Guyomard, D.; Bideau, J. L. Hybrid Silica−Polymer Ionogel Solid Electrolyte with Tunable Properties. *Adv. Energy Mater.* **2014**, *4* (8), 1301570.
(25) Chen, N.; Zhang, H.; Li, L.; Chen, R.; Guo, S. Ionogel Electrolytes for High-Performance Lithium Batteries: A Review. *Adv. Energy Mater.* **2018**, *8* (12), 1702675.
(26) Hyun, W. J.; Thomas, C. M.; Hersam, M. C. Nanocomposite Ionogel Electrolytes for Solid-State Rechargeable Batteries. *Adv. Energy Mater.* **2020**, *10* (36), 2002135.
(27) Hyun, W. J.; de Moraes, A. C. M.; Lim, J. M.; Downing, J. R.; Park, K. Y.; Tan, M. T. Z.; Hersam, M. C. High-Modulus Hexagonal Boron Nitride Nanoplatelet Gel Electrolytes for Solid-State Rechargeable Lithium-Ion Batteries. *ACS Nano* **2019**, *13* (8), 9664−9672.
(28) Hyun, W. J.; Thomas, C. M.; Luu, N. S.; Hersam, M. C. Layered Heterostructure Ionogel Electrolytes for High-Performance Solid-State Lithium-Ion Batteries. *Adv. Mater.* **2021**, *33* (13), 2007864.
(29) Lewandowski, A.; Świderska-Mocek, A. Ionic Liquids as Electrolytes for Li-Ion Batteries—An Overview of Electrochemical Studies. *J. Power Sources* **2009**, *194* (2), 601−609.
(30) Tokuda, H.; Hayamizu, K.; Ishii, K.; Susan, M. A. B. H.; Watanabe, M. Physicochemical Properties and Structures of Room Temperature Ionic Liquids. 2. Variation of Alkyl Chain Length in Imidazolium Cation. *J. Phys. Chem. B* **2005**, *109* (13), 6103−6110.
(31) Ishikawa, M.; Sugimoto, T.; Kikuta, M.; Ishiko, E.; Kono, M. Pure Ionic Liquid Electrolytes Compatible with a Graphitized Carbon Negative Electrode in Rechargeable Lithium-Ion Batteries. *J. Power Sources* **2006**, *162* (1), 658−662.
(32) Paillard, E.; Zhou, Q.; Henderson, W. A.; Appetecchi, G. B.; Montanino, M.; Passerini, S. Electrochemical and Physicochemical Properties of $Py_{14}FSI$-Based Electrolytes with LiFSI. *J. Electrochem. Soc.* **2009**, *156* (11), A891.
(33) Heist, A.; Lee, S.-H. Improved Stability and Rate Capability of Ionic Liquid Electrolyte with High Concentration of LiFSI. *J. Electrochem. Soc.* **2019**, *166* (10), A1860−A1866.
(34) Periyapperuma, K.; Arca, E.; Harvey, S.; Pathirana, T.; Ban, C.; Burrell, A.; Pozo-Gonzalo, C.; Howlett, P. C. High Current Cycling in a Superconcentrated Ionic Liquid Electrolyte to Promote Uniform Li Morphology and a Uniform LiF-Rich Solid Electrolyte Interphase. *ACS Appl. Mater. Interfaces* **2020**, *12* (37), 42236−42247.
(35) Kim, K. K.; Hsu, A.; Jia, X.; Kim, S. M.; Shi, Y.; Hofmann, M.; Nezich, D.; Rodriguez-Nieva, J. F.; Dresselhaus, M.; Palacios, T.; et al. Synthesis of Monolayer Hexagonal Boron Nitride on Cu Foil Using Chemical Vapor Deposition. *Nano Lett.* **2012**, *12* (1), 161−166.
(36) Schmitt, M. Slot Die Coating of Lithium-ion Battery Electrodes. Ph.D. Dissertaion, Karlsruhe Institute of Technology, Karlsruhe, Germany, 2015. https://d-nb.info/1100444181/34 (accessed 2021-02-03).
(37) N,N-dimethyl-formamide. *NIST Chemistry WebBook*. National Institute of Standards and Technology. https://webbook.nist.gov/chemistry/ (accessed 2021-06-25). (CAS Reg. No.: 68-12-2).
(38) Yamada, Y.; Wang, J.; Ko, S.; Watanabe, E.; Yamada, A. Advances and Issues in Developing Salt-Concentrated Battery Electrolytes. *Nat. Energy* **2019**, *4* (4), 269−280.
(39) Yang, X.; Jiang, M.; Gao, X.; Bao, D.; Sun, Q.; Holmes, N.; Duan, H.; Mukherjee, S.; Adair, K.; Zhao, C.; et al. Determining the Limiting Factor of the Electrochemical Stability Window for PEO-Based Solid Polymer Electrolytes: Main Chain or Terminal − OH Group? *Energy Environ. Sci.* **2020**, *13* (5), 1318−1325.
(40) Chen, X.; He, W.; Ding, L.-X.; Wang, S.; Wang, H. Enhancing Interfacial Contact in All Solid State Batteries with a Cathode-Supported Solid Electrolyte Membrane Framework. *Energy Environ. Sci.* **2019**, *12* (3), 938−944.
(41) Wu, J.; Rao, Z.; Cheng, Z.; Yuan, L.; Li, Z.; Huang, Y. Ultrathin, Flexible Polymer Electrolyte for Cost-Effective Fabrication of All-Solid-State Lithium Metal Batteries. *Adv. Energy Mater.* **2019**, *9* (46), 1902767.
(42) Wan, J.; Xie, J.; Kong, X.; Liu, Z.; Liu, K.; Shi, F.; Pei, A.; Chen, H.; Chen, W.; Chen, J.; et al. Ultrathin, Flexible, Solid Polymer Composite Electrolyte Enabled with Aligned Nanoporous Host for Lithium Batteries. *Nat. Nanotechnol.* **2019**, *14* (7), 705−711.
(43) Jiang, T.; He, P.; Wang, G.; Shen, Y.; Nan, C.-W.; Fan, L.-Z. Solvent-Free Synthesis of Thin, Flexible, Nonflammable Garnet-Based Composite Solid Electrolyte for All-Solid-State Lithium Batteries. *Adv. Energy Mater.* **2020**, *10* (12), 1903376.
(44) Sun, J.; Yao, X.; Li, Y.; Zhang, Q.; Hou, C.; Shi, Q.; Wang, H. Facilitating Interfacial Stability Via Bilayer Heterostructure Solid

Electrolyte Toward High-energy, Safe and Adaptable Lithium Batteries. *Adv. Energy Mater.* **2020**, *10* (31), 2000709.
(45) Huo, H.; Chen, Y.; Luo, J.; Yang, X.; Guo, X.; Sun, X. Rational Design of Hierarchical "Ceramic-in-Polymer" and "Polymer-in-Ceramic" Electrolytes for Dendrite-Free Solid-State Batteries. *Adv. Energy Mater.* **2019**, *9* (17), 1804004.
(46) Yu, D.; Pan, X.; Bostwick, J. E.; Zanelotti, C. J.; Mu, L.; Colby, R. H.; Lin, F.; Madsen, L. A. Room Temperature to 150 °C Lithium Metal Batteries Enabled by a Rigid Molecular Ionic Composite Electrolyte. *Adv. Energy Mater.* **2021**, *11* (12), 2003559.
(47) Zhang, M.; Zhang, A. M.; Chen, Y.; Xie, J.; Xin, Z.-F.; Chen, Y.-J.; Kan, Y.-H.; Li, S.-L.; Lan, Y.-Q.; Zhang, Q. Polyoxovanadate-Polymer Hybrid Electrolyte in Solid State Batteries. *Energy Storage Mater.* **2020**, *29*, 172−181.
(48) Yan, C.; Zhu, P.; Jia, H.; Du, Z.; Zhu, J.; Orenstein, R.; Cheng, H.; Wu, N.; Dirican, M.; Zhang, X. Garnet-Rich Composite Solid Electrolytes for Dendrite-Free, High-Rate, Solid-State Lithium-Metal Batteries. *Energy Storage Mater.* **2020**, *26*, 448−456.
(49) Yan, X.; Li, Z.; Wen, Z.; Han, W. Li/$Li_7La_3Zr_2O_{12}$/$LiFePO_4$ All-Solid-State Battery with Ultrathin Nanoscale Solid Electrolyte. *J. Phys. Chem. C* **2017**, *121* (3), 1431−1435.
(50) Cui, Y.; Liang, X.; Chai, J.; Cui, Z.; Wang, Q.; He, W.; Liu, X.; Liu, Z.; Cui, G.; Feng, J. High Performance Solid Polymer Electrolytes for Rechargeable Batteries: A Self-Catalyzed Strategy toward Facile Synthesis. *Adv. Sci.* **2017**, *4* (11), 1700174.
(51) Bi, Z.; Mu, S.; Zhao, N.; Sun, W.; Huang, W.; Guo, X. Cathode Supported Solid Lithium Batteries Enabling High Energy Density and Stable Cyclability. *Energy Storage Mater.* **2021**, *35*, 512−519.
(52) Wu, Q.; Yang, Y.; Chen, Z.; Su, Q.; Huang, S.; Song, D.; Zhu, C.; Ma, R.; Li, C. Dendrite-Free Solid-State Li Metal Batteries Enabled by Bifunctional Polymer Gel Electrolytes. *ACS Appl. Energy Mater.* **2021**, *4* (9), 9420−9430.

Recommended by ACS

Hybrid Artificial Solid Electrolyte Interphase with Dendrite-Free Lithium Deposition and High Ion Transport Kinetics
Donggun Kim, Ying Chen, *et al.*
NOVEMBER 15, 2022
ACS APPLIED MATERIALS & INTERFACES
READ

Electrode Interface Engineering in Lithium–Sulfur Batteries Enabled by a Trifluoroacetamide-Based Electrolyte
Liang He, Yanqing Lai, *et al.*
JULY 10, 2022
ACS APPLIED MATERIALS & INTERFACES
READ

High Voltage $LiCoO_2$ Cathodes with High Purity Lithium Bis(oxalate) Borate (LiBOB) for Lithium-Ion Batteries
Yaprak Subaşı and Semih Afyon
JULY 26, 2022
ACS APPLIED ENERGY MATERIALS
READ

A Competitive Solvation of Ternary Eutectic Electrolytes Tailoring the Electrode/Electrolyte Interphase for Lithium Metal Batteries
Wanbao Wu, Jiaheng Zhang, *et al.*
AUGUST 30, 2022
ACS NANO
READ

Get More Suggestions >

https://doi.org/10.1021/acsenergylett.2c00535
ACS Energy Lett. 2022, 7, 1558−1565